國立交通大學

應用數學系

碩士論文

兩個耦合雙細胞類神經網路的動態系統

Dynamics in coupled two two-cell Cellular Neural Network systems

研究生：劉玟毅

指導教授：林松山　博士

中華民國九十四年六月

兩個耦合雙細胞類神經網路的動態系統

Dynamics in coupled two two-cell Cellular Neural Network systems

研 究 生：劉玟毅　　Student：Wen-Yi Liu

指導教授：林松山　　Advisor：Song-Sun Lin

國 立 交 通 大 學

應 用 數 學 研 究 所

碩 士 論 文

A Thesis

Submitted to Institute of Applied Mathematics

College of Science

National Chiao Tung University

in Partial Fulfillment of the Requirements

for the Degree of

Master

in

Applied Mathematics

June 2005

Hsinchu, Taiwan, Republic of China

中 華 民 國 九 十 四 年 六 月

兩個耦合雙細胞類神經網路的動態系統

研究生：劉玟毅　　指導教授：林松山 博士

國立交通大學應用數學系（研究所） 碩士班

摘　　要

在本篇論文中，我們研究具有四個細胞之類神經網路模型的混沌行為，此模型可以視為兩個雙細胞類神經網路的組合，而且這兩個類神經網路之間是有交互影響的；如果我們只考慮其中一個類神經網路的話，這與 Zou & Nossek[19]以及楊定揮的博士論文[22]的情況是不一樣的，他們所考慮的模型是一個有平滑輸入函數的非自主性（non-autonomous）系統，而我們的模型是以片段型線性函數作為輸入函數的自主性（autonomous）系統，此輸入函數是跟細胞本身以及輸出函數有關係的。在某些參數範圍，我們找到形如高跟鞋的混沌吸引子（chaotic attractor）。為了研究四個細胞之類神經網路的分歧和混沌現象，我們使用快速傅利葉轉換（Fast Fourier Transform）與計算 Lyapunov 指數（Lyapunov exponent）等數值方法。此外，我們也發展出一套用來計算 Lyapunov 指數的演算法，而且這個演算法是同時適用於自主性與非自主性的系統。

關鍵字：細胞類神經網路、混沌、Lyapunov 指數。

Dynamics in coupled two two-cell Cellular Neural Network systems

Student: Wen-Yi Liu* Advisor: Dr. Song-Sun Lin†

Department of Applied Mathematics,
National Chiao-Tung University,
Hsin-Chu 30050, Taiwan

June 21,2005

Abstract

In this thesis we study the chaotic behavior of four-neuron cellular neural networks model, this model can be treated as the combination of two two-neuron cellular neural networks and there are interactions between these two neural networks. If we only consider one of them, this is different from the case in ZN-case[19] and T.H.Yang's Ph.D Thesis[22]. The model they considered is a non-autonomous system with smooth input function. The one we consider is an autonomous system with piecewise-linear input which is related to neuron itself and output function. In some parameters ranges, we find a ladyshoe-like chaotic attractor. The numerical methods employed are of Fast Fourier Transform and Lyapunov exponents to study the bifurcation and chaotic phenomena of four-neuron neural network. Furthermore, an algorithm for computing Lyapunov exponents which is both adapted for autonomous and non-autonomous system is developed.

Keywords: Cellular Neural Networks, CNN, chaos, lady's shoe, Lyapunov exponent.

*E-mail: wyliu.am92g@nctu.edu.tw
†E-mail: sslin@math.nctu.edu.tw.

誌　　謝

這篇論文的完成，必須感謝每一位曾經教導、協助與支持我的人。首先，非常感謝我的指導教授 林松山博士，這兩年來耐心的指導與勉勵，讓我得以順利完成此篇論文。另外，也要感謝學長 楊定揮博士耐心地教我數值分析的方法與技巧，以及每週和我討論作研究時所遇到的問題，並且提供適時的建議與協助，讓我能夠突破學習和研究的瓶頸，一步一步完成論文進度。謹此，致上我最誠摯的敬意與謝意。

接著，我要感謝我最親愛的父母親 劉建一先生與謝紅桃女士，在求學的每個階段裡，他們總是在背後默默地支持我、鼓勵我，讓我可以無後顧之憂的學習，朝著自己的理想邁進；還要感謝大姊、二姊、哥哥、嫂嫂和三姊，在我最需要幫助的時候，永遠是第一個伸出溫暖的雙手給我信心和力量，陪伴我渡過每次的人生考驗。謹此，獻上我最真誠、感恩的心，因為沒有他們，就沒有現在的我。

Contents

Abstract (in Chinese) i

Abstract (in English) ii

Acknowledgement (in Chinese) iii

Contents iv

1 Introduction 1

2 Numerical methods 7

3 Some numerical results: PART I 13

4 Some numerical results: PART II 28

5 Conclusions and future works 38

References 39

1 Introduction

1.1 Introduction to CNN and our works

Cellular Neural Networks(CNN) are complex dynamical systems described by a large set of coupled nonlinear ordinary differential equations. The original model was firstly introduced by Chua and Yang (see,e.g.,[1],[2],[3]), and recently researchers devoted to study the stability, patterns , spatial chaos and entropy of CNN (see,e.g.,[4],[5],[6],[7],[8],[9],[10],[11],[12],[13]). Following the development of technology, CNN have extensively applications in the area of image processing, pattern recognition, artificial intelligence and signal processing (see,e.g.,[14],[15],[16],[17],[18]).

Zou and Nossek discovered a chaotic attractor, so-called lady's shoe, in a two-neuron CNN with an anti-symmetric feedback template, a periodic input function (forcing term) and typical piecewise-linear output function (see,e.g.,[19],[20],[21]). Afterward Lin, Lin and Yang investigate the bifurcation and chaos of a two-neuron CNN with periodic inputs in a general situation, such as varying templates, amplitude and period (see,e.g.,[22]). Following their works in two-neuron CNN, this study concerns about the dynamics behavior of a four-neuron CNN consisting of two two-neuron CNN with mutual connection strength. In other words, we generalize our four-neuron CNN from two-neuron CNN. The model is the combination of two two-neuron subsystem, the connection strength depending on neuwon itself and output function. In this thesis we concentrate on the numerical experiment results and related computational analysis of chaotic phenomena.

Four main results for this thesis can be summarized as follows. Instead of piecewise-linear output function, we use sigmoid C^∞ function, for example, hyperbolic tangent function. We also observe a chaotic attractor. In addition to output function, we also use quasi-periodic function as input and this also causes chaotic behavior. The results are presented in subsection 3.1. The second one is a result about coupled four-neuron CNN, and Fast Fourier Transform and Lyapunov exponents are employed to analyze. This part

is in subsection 3.2 and discuss them in detail. Being different from the coupled CNN, the third one we consider the uncoupled multi-layer CNN and its dynamics, and we put it in section 4 alone. The last result is that we establish a complete algorithm for computing Lyapunov exponents, this helps us to explicitly determine whether a system is chaotic or not.

This thesis is organized as follows. In section 1, a brief introduction of CNN model is introduced. In section 2, we establish the algorithm for calculating Lyapunov exponents. And then show some interesting numerical computation results in section 3 and section 4. In section 5, we conclude in some remarks and address the future works.

1.2 Model description

In the following, a 1-dimensional CNN with four neurons described by a system of nonlinear ordinary differential equations is considered:

$$\begin{cases} \dot{x_1} &= -x_1 + p_1 y_1 + s_1 y_2 + r y_3 \ , \\ \dot{x_2} &= -x_2 + r_1 y_1 + p_1 y_2 \ , \\ \dot{x_3} &= -x_3 + p_2 y_3 + s_2 y_4 + s y_1 \ , \\ \dot{x_4} &= -x_4 + r_2 y_3 + p_2 y_4 \ , \end{cases} \tag{1.1}$$

where x_1, x_2, x_3 and x_4 present the voltages of the neurons, and the output function of a neuron is given as a piecewise-linear neuron-activation function

$$y_i = f(x_i) = \frac{1}{2}(|x_i + 1| - |x_i - 1|), \quad (i = 1, 2, 3, 4), \tag{1.2}$$

which is shown in Figure 1.

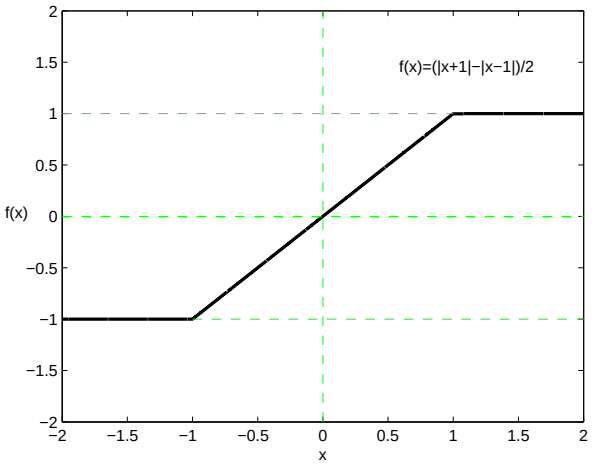

Figure 1. Piecewise-linear function $f(x) = \frac{1}{2}(|x+1|-|x-1|)$

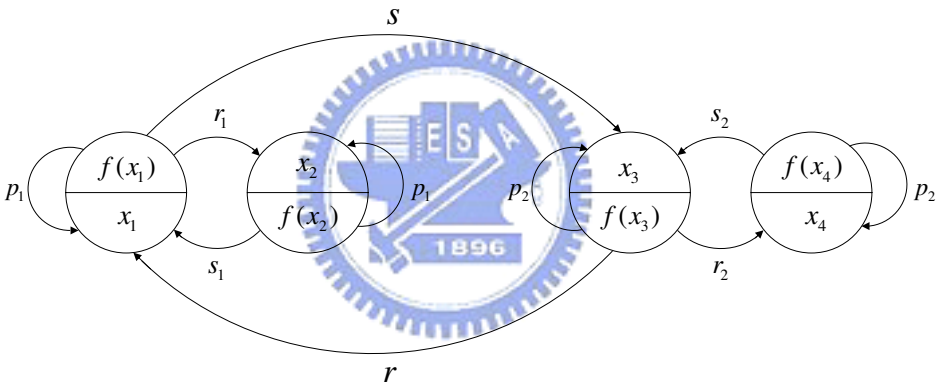

Figure 2. Our model: an autonomous four-neuron CNN

Here, as in two-neuron CNN model, two feedback templates $A_1 = [r_1, p_1, s_1]$ and $A_2 = [r_2, p_2, s_2]$ are considered. The internal state of A_1 and A_2 are denoted by x_1, x_2 and x_3, x_4, respectively. The parameters r and s are the connection strengths between A_1- and A_2-subsystem and denote $A = [r, 0, s]$ as the connection template.

Motivated by [19] and [22], as we mentioned above, (1.1) is regarded as a combination of two two-neuron subsystems. Without connection, these two subsystems are independent to each other. In order to have periodic cycles,

A_1 and A_2 are required to satisfy the following conditions:

$$p_1 > 1, \quad p_1 - 1 < r_1, \quad p_1 - 1 < -s_1 \tag{1.3}$$

$$\text{and} \quad p_2 > 1, \quad p_2 - 1 < r_2, \quad p_2 - 1 < -s_2 \tag{1.4}$$

respectively.

Since (1.1) involves eight parameters: $r_1, p_1, s_1, r_2, p_2, s_2, r$ and s, we begin with the study of anti-symmetric templates A_1 and A_2. The study is divided into three cases for our discussion.

(i) When $s = 0,\ r = 0$, these two subsystems generate respectively stable limit cycles Λ_{A_1} and Λ_{A_2}.

(ii) When $s = 0,\ r > 0$, A_2-subsystem will not be affected by A_1-subsystem. The periodic solution generated by A_2-subsystem will be the input function of A_1-subsystem. Comparing with ZN-case, our system is autonomous with input function ry_3. For some r, (1.1) has chaotic attractor later.

(iii) When $s \sim 0, r > 0$, not only A_2-subsystem influences A_1-subsystem but also A_1-subsystem influenced A_2-subsystem. Numerical results suggest that chaotic attractor is sensitive dependence on parameters. In other words the dynamic behaviors vary with the varied parameter s. For instance, if s is close to zero the chaotic attractor still exists; if s is larger than a critical number the chaotic attractor disappears.

These related numerical results are presented in subsection 3.2.

1.3 Preliminaries

We first recall some useful notions. An isolated periodic solution is called a *limit cycle*. Positive Lypunov exponent is a criterion for chaotic attractor. The Lyapunov exponent of a smooth map f from $\mathbb{R}^m$ to $\mathbb{R}^m$ is defined as follows, [25].

Definition 1.1. For a smooth map f on $\mathbb{R}^m$, let $J_n = Df^n(v_0)$, and for $k = 1, \ldots, m$, let R_k^n be the length of k-th longest orthogonal axis of the ellipsoid J_nU for an orbit with initial point v_0. Then R_k^n measures the contraction or expansion near the orbit of v_0 is defined by

$$\lambda_k = \lim_{n\to\infty} \log((R_k^n)^{1/n}), \tag{1.5}$$

if the limit exists.

With the definition of Lyapunov exponent, chaotic orbit can be introduced.

Definition 1.2. Let $\phi_t(x_0)$ be a solution of $\dot{x} = f(x)$ with initial condition $x(0) = x_0$, where $x_0 \in \mathbb{R}^m$. We say the orbit $\phi_t(x_0)$ is chaotic if the following conditions hold:

(i) $\phi_t(x_0)$ is bounded, for $t \geq 0$;

(ii) $\phi_t(x_0)$ has at least one positive Lyapunov exponent; and

(iii) The ω-limit of $\phi_t(x_0)$ is not periodic and does not consist solely of equilibrium points, or solely of equilibrium points and connecting arcs.

Next, we state some symmetric property of the solutions of system (1.1) with initial condition

$$(x_1(0), x_2(0), x_3(0), x_4(0)) = (\eta_1,\ \eta_2,\ \eta_3,\ \eta_4). \tag{1.6}$$

Proposition 1.3. Assume $f(-x) = -f(x)$. When $r = s = 0$ and both templates A_1 and A_2 are anti-symmetric (i.e., $s_1 = -r_1$,$s_2 = -r_2$). If $(x_1(t), x_2(t), x_3(t), x_4(t)$ is a solution of (1.1), then $(x_2(t), -x_1(t), x_4(t), -x_3(t)$ is also a solution.

Proof. When $r = s = 0$, $s_1 = -r_1$ and $s_2 = -r_2$.
Let $(w_1(t), w_2(t), w_3(t), w_4(t)) = (x_2(t), -x_1(t), x_4(t), -x_3(t))$. Then, we have

$$\begin{cases} \dot{w}_1 &= -w_1 + p_1 f(w_1) + s_1 f(w_2)\ , \\ \dot{w}_2 &= -w_2 + r_1 f(w_1) + p_1 f(w_2)\ , \\ \dot{w}_3 &= -w_3 + p_2 f(w_3) + s_2 f(w_4)\ , \\ \dot{w}_4 &= -w_4 + r_2 f(w_3) + p_2 f(w_4)\ , \end{cases} \tag{1.7}$$

which implies that

$$\begin{cases} \dot{x_2} &= -x_2 + r_1 f(x_1) + p_1 f(x_2) \ , \\ \dot{x_1} &= -x_1 + p_1 f(x_1) + s_1 f(x_2) \ , \\ \dot{x_4} &= -x_4 + r_2 f(x_3) + p_2 f(x_4) \ , \\ \dot{x_3} &= -x_3 + p_2 f(x_3) + s_2 f(x_4) \ , \end{cases} \tag{1.8}$$

since $f(-x_i) = -f(x_i)$ and i=1,2,3,4. Hence, $(x_2(t), -x_1(t), x_4(t), -x_3(t)$ is also a solution. The proof is complete. □

2 Numerical methods

In this section, we introduce some numerical methods which include the computation of trajectory, Poincaré section, Fast Fourier Transform (FFT) and Lyapunov exponents. We also provide a complete algorithm for computing Lyapunov exponents in subsection 2.2.

2.1 Introductory to some numerical methods

trajectory

Since the CNN model considered is a system of differential equations, fourth-order Runge-Kutta numerical integration method (R.K-45) is used with fixed step size h=0.001 and graphic libraries in MATLAB language.

Poincaré section

If the input function in the system is periodic with period T, the time-T map is our Poincaré section. For instance, in two-neuron networks system, suppose that the period of the input function is T and the step size is $\triangle\ t$, we can take sample points per $\frac{T}{\triangle t}$ as Poincaré section. However, for higher dimensional system, the method has to be modified. For instance, in four-neuron system, the method used here is that we take a point and a direction to determine a hyper-plane, and this hyper-plane helps us to reduce to three-dimensional space and then we project onto x_1-x_2 plane directly.

FFT

FFT is a classical algorithm which transforms time-domain into frequency-domain. It helps to analyze the solution waveform. As for a chaotic attractor, its FFT has a broad-band. In practical numeric, we call the built-in procedure "fft" in MATLAB for our works.

Lyapunov exponent

The Lyapunov exponents are computed by averaging the eigenvalues of derivative matrix $DF(\eta 1, \eta 2)$ on every point of time-1 map. During the process of computation, if the relative error is less than 1×10^{-4}, the convergent condition is attended. Furthermore, to accelerate the rate of convergence, the first 1×10^5 steps in the numerical integration is ignored.

2.2 Algorithm for Lyapunov exponents

In this section the Lyapunov exponent is established a complete algorithm. The n-dim. autonomous differential equation is considered.

$$\dot{\mathbf{x}} = f(\mathbf{x}) \text{ , where } \mathbf{x} \in \mathbb{R}^n. \tag{2.1}$$

i.e.,

$$\begin{cases} \dot{x_1} &= f_1(x_1, x_2, \cdots, x_n) \ , \\ \dot{x_2} &= f_2(x_1, x_2, \cdots, x_n) \ , \\ \vdots &= \quad \vdots \\ \dot{x_n} &= f_n(x_1, x_2, \cdots, x_n) \ . \end{cases} \tag{2.2}$$

In general, the non-autonomous differential equation $\dot{\mathbf{x}} = f(t, \mathbf{x})$, can be studied as

$$\begin{cases} \dot{\mathbf{x}} &= f(t, \mathbf{x}) \ , \\ \dot{t} &= 1 \ . \end{cases} \tag{2.3}$$

For clarity, we divide into several steps and explain them in each step.

Description of algorithm

Step 1

In the first step, since the Lyapunov exponents measure the per-iterate changing rates of separation or expansion from the current orbit along each orthogonal directions, we recall the time-T map of a flow $F_T(v)$ at first. Note that the flow $F_T(v)$ is the point which the orbit with initial condition v arrives at after T time units and v satisfies $\dot{v} = f(v)$. Then the Lyapunov exponents of the flow $F_T(v)$ are defined to be the Lyapunov exponents of the associated time-1 map.

Step 2

From the definition of the Lyapunov exponents we need to know the derivative of the time-1 map $F_1(v)$ with respect to the initial value v.

Step 3

In the third step, we arise a variational equation of the original differential equations (2.1) in order to solve out, $DF_1(v)$, the solution of the variational equation. We solve the n-variable differential equation and the variational equation simultaneously and obtain the solution named $\mathbf{y}$ which is a $(n^2 + n) \times 1$ column vector. We denote $\mathbf{y}(k)$ to be the k-th element of $\mathbf{y}$ and also denote the subscript i to be the i-th element of any column vector mentioned in algorithm. We know the former n components of $\mathbf{y}$ is just the solution of our n-dimensional differential equations and the rest n^2 components of $\mathbf{y}$ can be rearranged as the $n \times n$ square matrix named V.

Step 4

After multiplying V and W, we regard VW as a new matrix V. By Gram-Schmidt orthogonal process, we obtain the Lyapunov exponents applying the definition of the Lyapunov exponents in the first step. Furthermore, we ask the basis matrix W in every recursive process be the normal basis so we orthonomalize these orthogonal basis. In addition, as the maximum iteration number is attended or the result is convergent under our tolerance then the process stops.

Algorithm for Lyapunov exponent

Input $N_{\text{iteration}}$, $N_{\text{maximum iteration}}$, M, $\triangle t$, T, dimension, W

$\triangle t \leftarrow 0.01$ (step size)

$T \leftarrow 1$

$\varepsilon \leftarrow 10^{-4}$

dimension $\leftarrow n$

$W \leftarrow I_{n\times n}$

for $N_{\text{iteration}} = 1, 2, \ldots, M$ **do**

$t \leftarrow 0 : \triangle t : T$

call SolveODE$(t, \tilde{\mathbf{x}})$

output $t, \mathbf{y}$

$$V \leftarrow \begin{bmatrix} \mathbf{y}(n+1) & \mathbf{y}(2n+1) & \cdots & \mathbf{y}(n^2+1) \\ \mathbf{y}(n+2) & \mathbf{y}(2n+2) & \cdots & \mathbf{y}(n^2+2) \\ \vdots & \vdots & \ddots & \vdots \\ \mathbf{y}(n+n) & \mathbf{y}(2n+n) & \cdots & \mathbf{y}(n^2+n) \end{bmatrix}$$

$V \leftarrow VW$

call GramSchmidt(V)

output V

for each dimension from 1 to n

Lyapunov $\leftarrow$ Lyapunov$+\log \|V\|$

end

result $\leftarrow \dfrac{\text{Lyapunov}}{N_{\text{iteration}}T}$

for each dimension from 1 to n

$W \leftarrow \dfrac{V}{\|V\|}$

end

$$\mathbf{x} \leftarrow \begin{bmatrix} \mathbf{y}(1) \\ \mathbf{y}(2) \\ \vdots \\ \mathbf{y}(n^2+n) \end{bmatrix}$$

if $N_{\text{iteration}} > N_{\text{maximum iteration}}$

then stop: Maximum iteration is attended.

if $\|\text{result}_{\text{new}} - \text{result}_{\text{old}}\|_\infty < \varepsilon$

then stop: Result is convergent.

$N_{\text{iteration}} \leftarrow N_{\text{iteration}} + 1$

$\text{result}_{\text{old}} \leftarrow \text{result}_{\text{new}}$

end

procedure SolveODE($t, \tilde{\mathbf{x}}$)

$$\begin{bmatrix} x_1 \\ x_2 \\ \vdots \\ x_n \end{bmatrix} \leftarrow \begin{bmatrix} \mathbf{X}(1) \\ \mathbf{X}(2) \\ \vdots \\ \mathbf{X}(n) \end{bmatrix}$$

$$Q_{n\times n} \leftarrow \begin{bmatrix} \mathbf{X}(n+1) & \mathbf{X}(2n+1) & \cdots & \mathbf{X}(n^2+1) \\ \mathbf{X}(n+2) & \mathbf{X}(2n+2) & \cdots & \mathbf{X}(n^2+2) \\ \vdots & \vdots & \ddots & \vdots \\ \mathbf{X}(n+n) & \mathbf{X}(2n+n) & \cdots & \mathbf{X}(n^2+n) \end{bmatrix}$$

$$\begin{bmatrix} dx_1 \\ dx_2 \\ \vdots \\ dx_n \end{bmatrix} \leftarrow \begin{bmatrix} f_1(x_1, x_2, \cdots, x_n) \\ f_2(x_1, x_2, \cdots, x_n) \\ \vdots \\ f_n(x_1, x_2, \cdots, x_n) \end{bmatrix}$$

$$J_{n\times n} \leftarrow \begin{bmatrix} \frac{\partial f_1}{\partial x_1} & \frac{\partial f_1}{\partial x_2} & \cdots & \frac{\partial f_1}{\partial x_n} \\ \frac{\partial f_2}{\partial x_1} & \frac{\partial f_2}{\partial x_2} & \cdots & \frac{\partial f_2}{\partial x_n} \\ \vdots & \vdots & \ddots & \vdots \\ \frac{\partial f_n}{\partial x_1} & \frac{\partial f_n}{\partial x_2} & \cdots & \frac{\partial f_n}{\partial x_n} \end{bmatrix}$$

$$\begin{bmatrix} dx_{n+1} & dx_{2n+1} & \cdots & dx_{n^2+1} \\ dx_{n+2} & dx_{2n+2} & \cdots & dx_{n^2+2} \\ \vdots & \vdots & \ddots & \vdots \\ dx_{n+n} & dx_{2n+n} & \cdots & dx_{n^2+n} \end{bmatrix} \leftarrow J_{n\times n}Q_{n\times n}$$

$$\tilde{\mathbf{x}} \leftarrow \begin{bmatrix} dx_1 \\ dx_2 \\ \vdots \\ dx_n \\ dx_{n+1} \\ dx_{n+2} \\ \vdots \\ dx_{n^2+n} \end{bmatrix}$$

$\mathbf{y} \leftarrow \text{ode45}(t, \tilde{\mathbf{x}})$

return

procedure GramSchmidt(V)

Input V

$\hat{V} \leftarrow V$

$m \leftarrow$ the column number of V

for $i = 1, 2, \ldots, m$ **do**

$V^{(i)} \leftarrow \hat{V}^{(i)}$

for $j = 1, 2, \ldots, i-1$ **do**

$$V^{(i)} \leftarrow V^{(i)} - \frac{(\hat{V}^{(i)})^t \, V^j}{\|V^j\|^2} V^j$$

end

end

3 Some numerical results: PART I

Since CNNs are large-scale nonlinear dynamical systems, it is not surprising that they may exhibit a complex dynamic behavior, including chaos. The purpose of this section is to show that complex dynamics occur even in very simple CNN structures. In this section, we take the two-neuron and four-neuron CNN as our examples and the chaotic attractor in each case is discovered. The algorithm developed in Section 2 and Fast Fourier Transform (FFT) are also applied in order to make further analysis. The numerical results will be presented in subsection 3.1 and subsection 3.2 respectively.

3.1 A new type of chaotic attractor in two-neuron CNN with periodic inputs

In the beginning of this investigation, we try two-neuron CNN model ZN-case i.e., the output function is piecewise-linear function, and input function is a periodic function $\sin(\frac{2\pi}{T}t)$. When template $A = [1.2, 2, -1.2]$, input amplitude $r = 4$ and input period $T = 4$, numerical results ensure that a chaotic attractor with shape of lady's shoe occurs. A broad range of these parameters A, r and T are investigated in [22].

From the previous results, a natural question arises: if the output function or input function is varied, is there still a chaotic attractor? In typical CNN models, the output function is chosen to be a piecewise-linear. Instead of piecewise-linear output function we try hyperbolic tangent function. To be concrete, we write down the modified models as follow.

$$\begin{cases} \dot{x_1} &= -x_1 + p_1 y_1 + s_1 y_2 + r\sin(\frac{2\pi}{T}t) \ , \\ \dot{x_2} &= -x_2 + r_1 y_1 + p_1 y_2 \ , \end{cases} \tag{3.1}$$

where the output function is a C^∞, sigmoidal neuron-activation function (cf. Figure. 3)

$$y_i = f(x_i) = \tanh(mx_i), i = 1, 2. \tag{3.2}$$

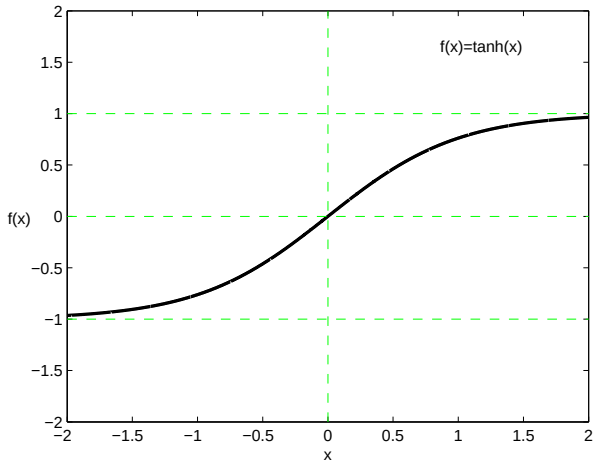

Figure 3. Hyperbolic tangent function $f(x)$=tanh(x)

The parameter $m = f'(0)$, the slope of curve, will play an important role in this case. By solving (3.1) with the following parameter setting:

$$r_1 = 1.2,\ p_1 = 2,\ s_1 = -1.2,\ r = 4,\ T = 4,\ m = 1.5 \tag{3.3}$$

and initial condition $(x_1(0), x_2(0)) = (0.1, 0.1)$, a chaotic attractor similar to ZN-case can be observed numerically (cf. Figure 4).

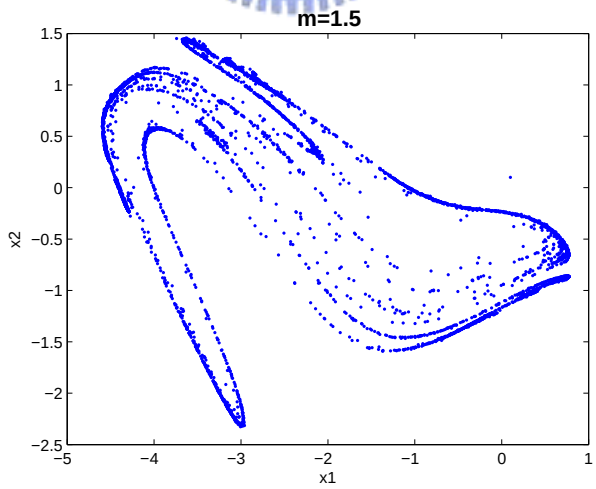

Figure 4. Cross-section for the trajectory of x_1 and x_2 when m=1.5

Next we apply the algorithm for calculating Lyapunov exponents. Input the parameter set (3.3), and the Lyapunov exponents of the system (3.1) are calculated as

$$\begin{cases} \lambda_1 &= 0.0617 \\ \lambda_2 &= -0.4597\ . \end{cases} \tag{3.4}$$

The largest Lyapunov exponents is greater than zero (even greater than 0.02), and this ensures that this attractor is chaotic.

When m varies from 0.5 to 2.5, the Lyapunov exponents of system is recorded as in Figure 5. It is clear that there are ranges of m exhibit chaotic attractor.

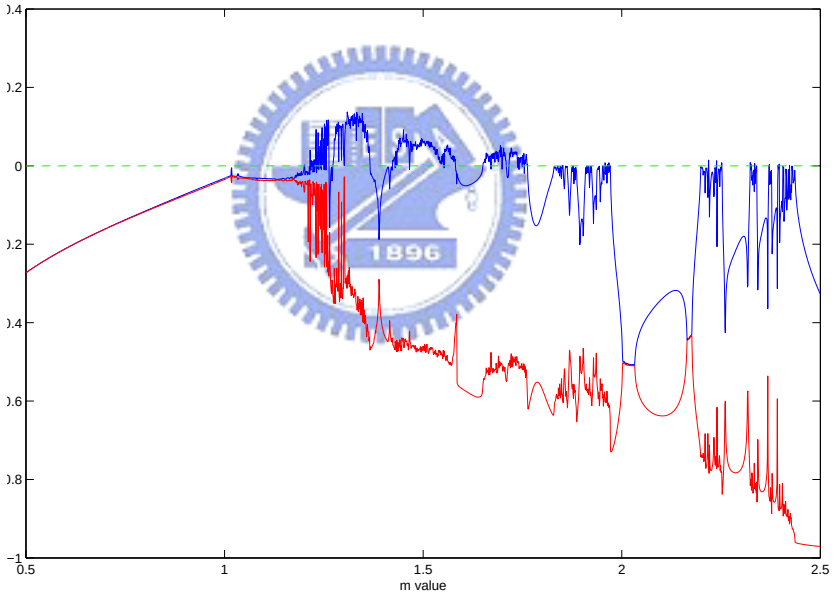

Figure 5. Lyapunov exponents diagram when m varies from 0.5 to 2.5

Finally, we make two remarks about the modified two-neuron network model (3.1), (3.2).

Remark 3.1. If the input function is replaced by other periodic function, for example $\cos(\frac{2\pi}{T}t)$, then the results are similar.

Remark 3.2. When the output function is hyperbolic tangent function, m is a crucial value. Compare with ZN-case, the slope of the piecewise-linear function evaluated at the origin is 1, while the slope of the hyperbolic tangent function evaluated at the origin is 1.5 .

Recall the setting of [19] and [22], and the input function is chosen to be sine function. In the rest part of subsection 1, the model we considered originates from ZN-case with piecewise-linear output function. Nevertheless, we add several periodic perturbation to the input function-sine function and the perturbed input function is of the form:

$$r\sin(\frac{2\pi}{T_1}t) + \varepsilon\sin(\frac{n\pi}{T_2}t), \tag{3.5}$$

where we request $n \geq 3$.

Under the following setting: $r = 4, T_1 = 4, \varepsilon = 1, n = 5, T_2 = 2$, the waveform of the periodic perturbed input function is shown in Figure 6.

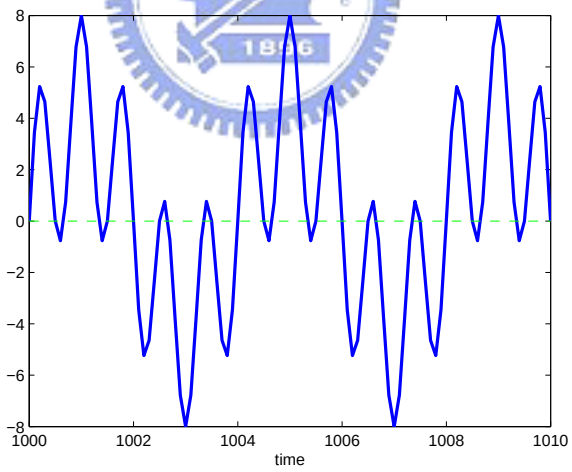

Figure 6. The input function: periodic perturbed sine function

We find its trajectory of solution is smooth but tremble. After taking appropriate Poincaré-section, a chaotic attractor can be observed (cf. Figure 7).

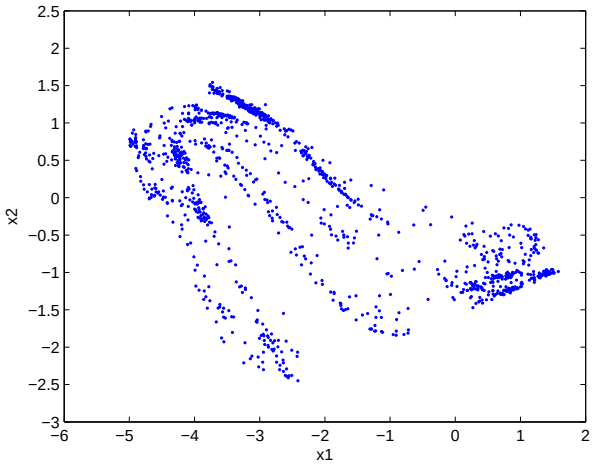

Figure 7. a chaotic attractor like lady's shoe

Again, apply the algorithm for calculating Lyapunov exponents and the Lyapunov exponents of the perturbed system are calculated as

$$\begin{cases} \lambda_1 &= 0.1064 \\ \lambda_2 &= -0.3805\ . \end{cases} \tag{3.6}$$

Hence the attractor in Figure 7 is exactly chaotic

Before any periodic perturbation is added, T_1 is the only period. Once we add periodic perturbation, the input function becomes from single-periodic to quasi-periodic and the system involves eight parameters: $r_1, p_1, s_1, r, T_1, \varepsilon, n$ and T_2. For brevity, we hold the other seven parameters fixed and vary T_2 only. Set $[r_1, p_1, s_1] = [1.2, 2, -1.2], r = 4, T_1 = 4, \varepsilon = 1, n = 5$, and let T_2 runs from 1 to 10, and further study the effect of the external period T_2 upon the system. The Lyapunov exponents are calculated in the following table as T_2 varies from 1 to 10.

T_1	T_2	λ_1	λ_2
4	1	0.01095	-0.45450
4	2	0.10638	-0.38051
4	3	-0.08864	-0.36511
4	4	-0.03669	-0.54255
4	5	-0.05543	-0.57615
4	6	-0.27744	-0.80849
4	7	-0.12011	-0.65675
4	8	-0.19732	-0.64681
4	9	-0.07363	-0.46564
4	10	-0.12908	-0.34245

Table 1. The Lyapunov exponents for fixed $T_1 = 4$ with respect to varying T_2

Remark 3.3. The above data indicates that to produce a chaotic attractor, the period of perturbation cannot exceed the period of original input function, otherwise, the chaotic attractor will disappear at once. Moreover, if ones choose suitable parameters then chaotic attractor will be preserved under small periodic perturbation.

3.2 The dynamic behavior of four-neuron CNN with nonzero connection strength

It is well-known that the templates, output function and input function play important roles in CNN models. To simplify our discussion later, the templates are fixed in later discussions. Before analyzing the dynamic behavior of (1.1), we need to generate the periodic solutions for each subsystem without connection strength. Moreover the periodic solution is related to the template closely, in fact, template $A = [r, 0, s]$ governs the connection strength between A_1-subsystem and A_2-subsystem. Motivated by two-neuron CNN, the templates A_1 and A_2 we select are also anti-symmetric. We choose $A_1 = [r_1, p_1, s_1] = [1.2, 2, -1.2]$ to generate a periodic solution with period about 17 and choose $A_2 = [r_2, p_2, s_2] = [2.9, 1.7, -2.9]$ to generation a periodic solution with period about 4. Figure 8 and Figure 9 show the periodic solutions for A_1-subsystem and A_2-subsystem.

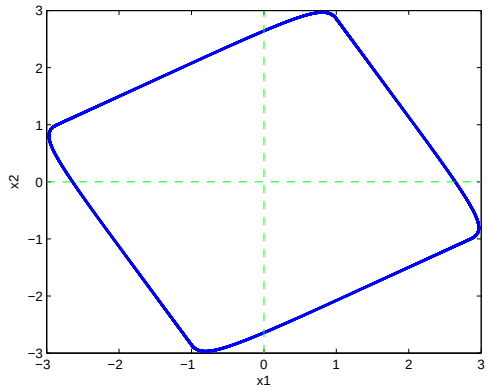

Figure 8. Periodic solution Λ_{A_1} for A_1-subsystem, $T_{A_1} = 17$

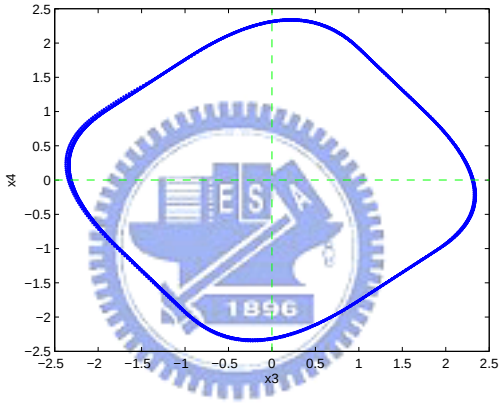

Figure 9. Periodic solution Λ_{A_2} for A_2-subsystem, $T_{A_2} = 4$

In the following we hold the templates A_1 and A_2 fixed and study the effect of connection strength upon the system (1.1). For clarity we divide into three cases for discussion.

Case 1: $s = 0, r = 0$

When s and r are both equal to zero, it means that there is no any relations between A_1-subsystem and A_2-subsystem. At this time the dynamic behavior is trivial since the trajectory of (1.1) is only the periodic solution. As for the existence and uniqueness of two-neuron networks system, this work was done by C.-H. Hsu,et al. in 2004. Delicate proof can be founded in [23], and their

work ensures that the periodic solution in individual subsystem is existent and unique.

Case 2: $s = 0, r > 0$

Once the periodic solution is generated in individual subsystem, let $s = 0$ and enlarge r. At this moment in time, the A_2-subsystem starts to influence A_1-subsystem; as far as the A_1-subsystem, $ry3$ is the only input function and its waveform is shown in Figure 10. If we just consider A_1-subsystem, this is back to the two-neuron CNN case. Notice that our input function "$ry3$" contains no other independent variable, so A_1-subsystem is an autonomous system. Moreover, the most difference between A_1-subsystem and ZN-case is that $ry3$ is not differentiable in some points but $r\sin(\frac{2\pi}{T}t)$ is differentiable everywhere.

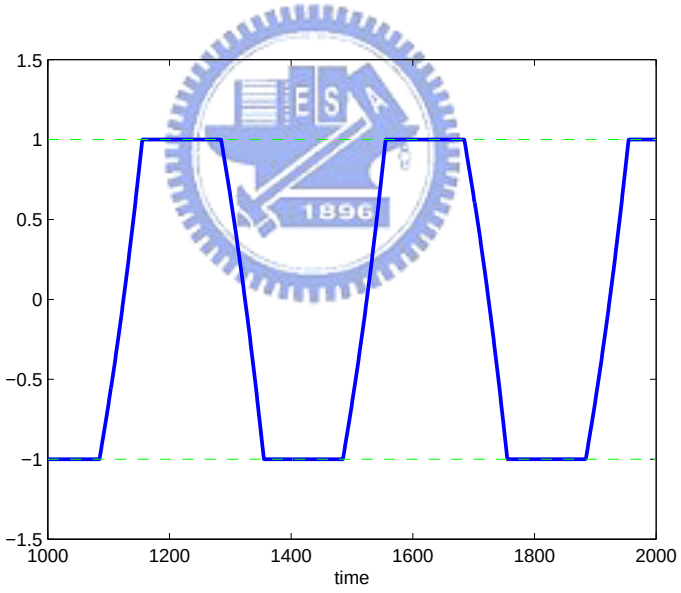

Figure 10. Waveform of ry_3

Numerically, keep $r_1, p_1, s_1, r_2, p_2, s_2$ and $s = 0$ and then increase r-value to drive the periodic solution Λ_{A_1} by means of the $ry3$-term. As we take r-value from 0.01 to 3.40, the cross-sections are nothing more than equilibrium, periodic solution and quasi-periodic solution. When r is near 3.50, a

ladyshoe-like chaotic attractor arises after taking Poincaré section and projecting onto x_1-x_2 plane. Figure 11 shows the chaotic attractor and its Lyapunov exponents are

$$\begin{cases} \lambda_1 &= 0.0755 \\ \lambda_2 &= -0.3518 \\ \lambda_3 &= -0.0131 \\ \lambda_4 &= -0.7894 \end{cases} \tag{3.7}$$

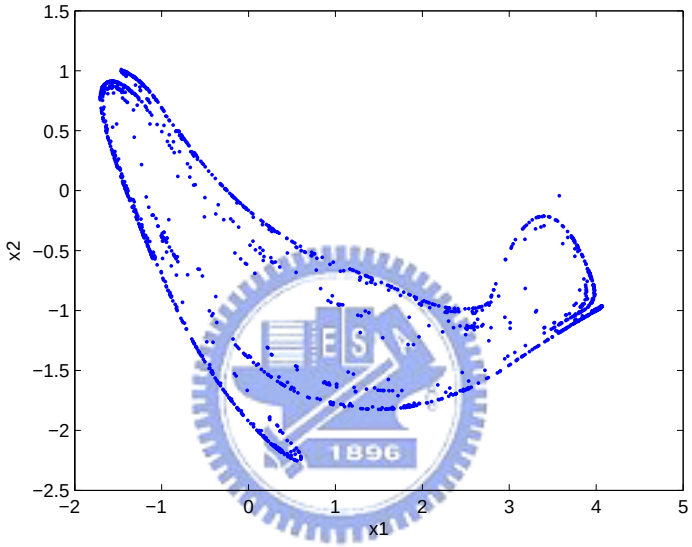

Figure 11. The chaotic attractor when $r = 3.5$,$s = 0$

Under the setting of $s = 0$, the Lyapunov exponents are calculated from $r = 3.0$ to $r = 4.0$ and recorded in the following diagram (cf. Figure 12) and table list (cf. Table 2).

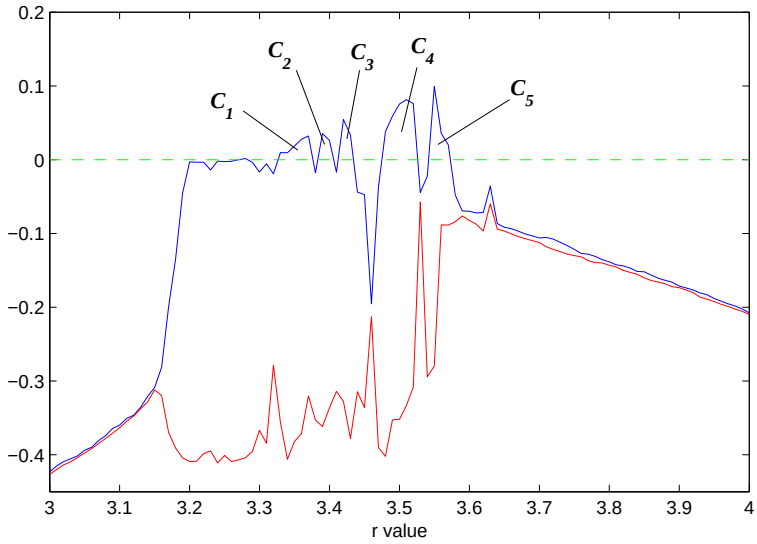

Figure 12. The Lyapunov exponents diagram for the four-neuron CNN when $s = 0$ and $r = 3.0 \sim 4.0$

Table 2. Five chaotic regions when $s = 0$

regions	range of parameter r
C_1	[3.33,3.37]
C_2	[3.39,3.40]
C_3	[3.42,3.43]
C_4	[3.48,3.52]
C_5	[3.55,3.57]

Here we call the region where its Lyapunov exponent is positive "chaotic region" and call the region where its Lyapunov exponent is negative "window region". In Table 2, we write capital C in short to stand for "Chaotic". Then the largest Lyapunov exponent that is close to or above zero is recorded in regions C_1, C_2, C_3, C_4 and C_5, and the others are window regions except for these five chaotic regions. In the following we present the Poincaré section of the trajectory in each chaotic region (see Figure 13(a)-(e)).

Remark 3.4. In case 2, if we replace the output function with the hyperbolic tangent function and m is setting around 1.5, we will have the similar dynamic result so we omit it here.

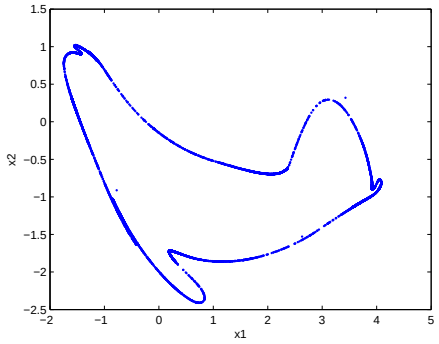

(a) $r = 3.369 \in C_1$

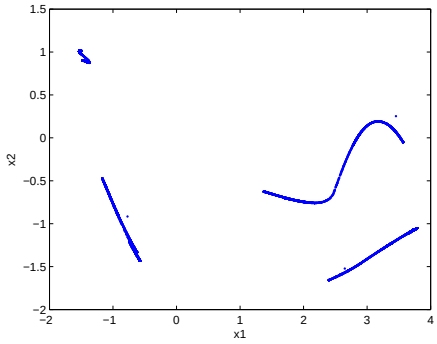

(b) $r = 3.395 \in C_2$

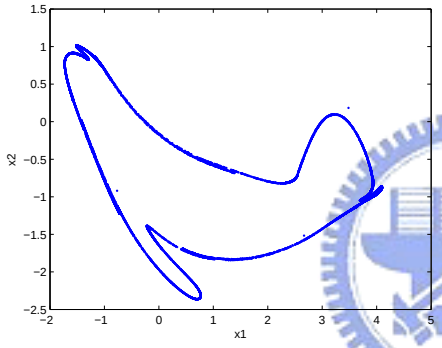

(c) $r = 3.421 \in C_3$

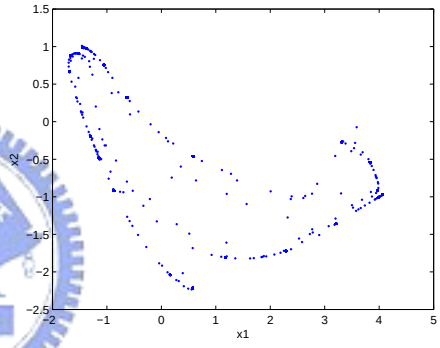

(d) $r = 3.510 \in C_4$

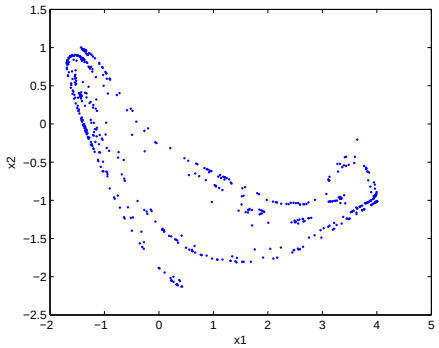

(e) $r = 3.552 \in C_5$

Figure 13. Some typical Poincaré section in chaotic regions, $s = 0$

Case 3: $s \sim 0, r > 0$

In case 2, we have found a chaotic attractor when $r = 3.5$, and proceed to let A_1-subsystem starts to influence A_2. To see what range a chaotic attractor still exists in, assume that s is nonzero, small enough(either positive or negative) and r is positive here. In this case, it is worth to notice that this chaotic attractor is sensitively dependent on the choice of the parameters. For example, when we fix $r = 3.50$, and s takes a value from 0.01 to 0.39, a ladyshoe-like chaotic attractor still exists but when s value is greater than 0.40, the chaotic attractor disappears and the trajectory asymptotically converges to a limit cycle or a quasi-periodic solution. On the other hand, keep the templates A_1, A_2 constant and fixed $s = 0.01$, when r takes a value from 3.45 to 3.59, a ladyshoe-like chaotic attractor emerges and when r exceeds 3.60, the chaotic attractor disappear and the trajectory asymptotically converges to a limit cycle.

The Lyapunov exponents diagram for fixed r and varying s are shown below (cf. Figure 14). In order to investigate the effect of the parameters r, s upon the chaotic attractor, the strategy is that hold one parameter fixed and vary the other one. In the first sample, fix $r = 3.50$ and vary s from -0.3 to 0.3 and list their Lyapunov exponents (when s is negative)in the table in detail (cf. Table 3).

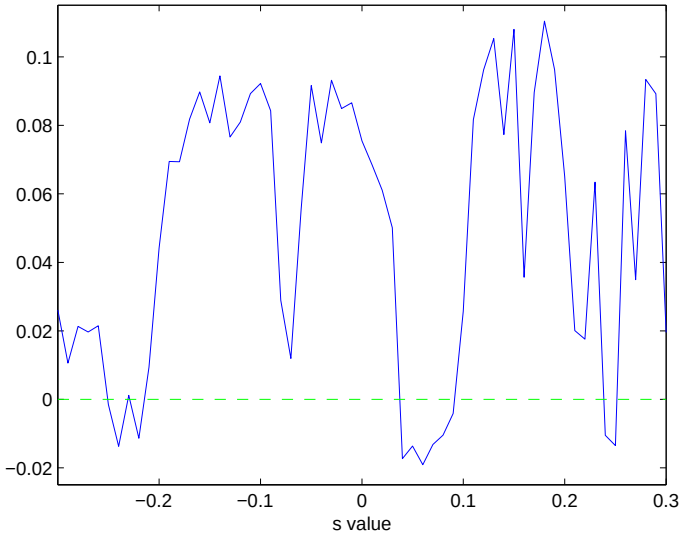

Figure 14. The Lyapunov exponents diagram for the four-neuron CNN when $r = 3.5$ and $s = -0.3 \sim 0.3$

r	s	λ_1	λ_2	λ_3	λ_4
3.50	-0.01	0.086595	-0.016514	-0.33726	-0.79049
3.50	-0.05	0.091612	-0.014737	-0.32491	-0.78995
3.50	-0.10	0.092231	-0.012774	-0.32857	-0.79027
3.50	-0.15	0.080732	-0.007268	-0.28292	-0.79172
3.50	-0.20	0.044199	-0.013886	-0.25791	-0.78829
3.50	-0.25	-0.001502	-0.006178	-0.24749	-0.78840
3.50	-0.30	0.026132	-0.011913	-0.26151	-0.78659

Table 3. The Lyapunov exponents for fixed $r = 3.50$ with respect to varying s ($s < 0$)

In the second sample, fix $s = 0.1$ and vary r from 3.20 to 3.70, and calculate the Lyapunov exponents for each parameter pair. About the largest Lyapunov exponent diagram when $s = 0.1$ and r=3.20 $\sim$ 3.70 are shown in Figure 15.

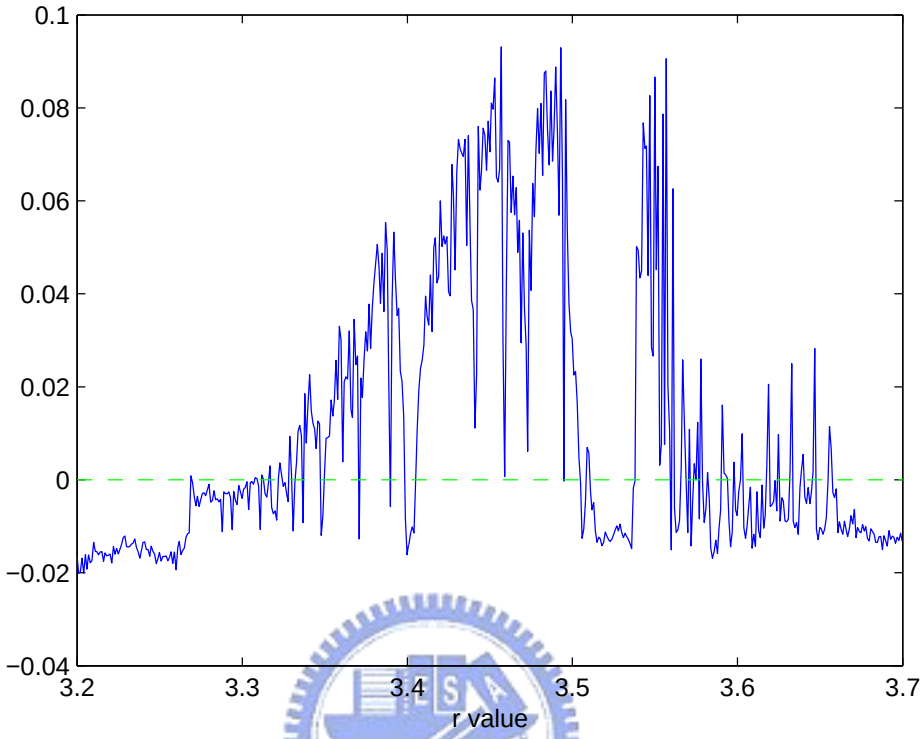

Figure 15. The largest Lyapunov exponents diagram for the four-neuron CNN when $s = 0.1$ and $r = 3.20 \sim 3.70$

Aimed at the case $s \sim 0$ and $r > 0$, we apply the Fast Fourier Transform to obtain more information about the behavior of the system (1.1) and focus on the largest 1 mode in FFT. Fixed $s \sim 0$, there are five chaotic regions and the others are windows regions. We apply the FFT in the windows region $(0, 3.2)$ and find the range $r \in (0, 1)$ of the windows region of periodic solutions form a devil's staircase. When $s = 0$ and $s = 0.5$ there are devil's staircase in both cases. See the following two figures.

(i) Let $s = 0$, r goes from 0 to 1 with step size 0.001;

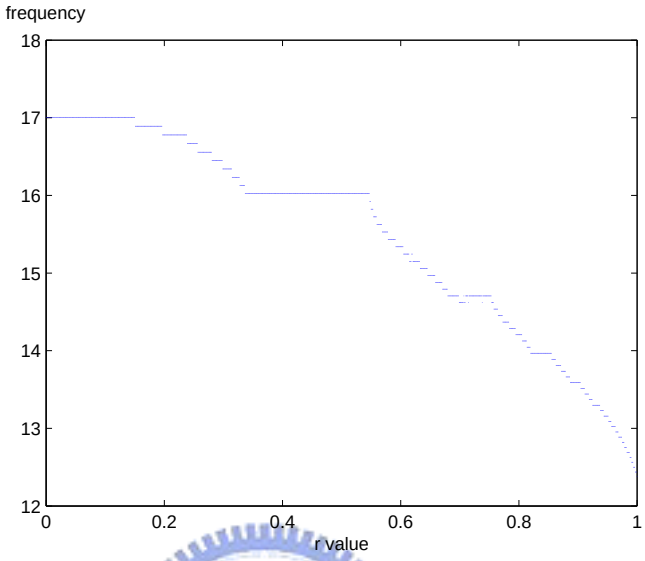

Figure 16. Devil's staircase-like function when $s = 0$ and $r \in (0, 1)$

(ii) Let $s = 0.5$, r goes from 0 to 1 with step size 0.001;

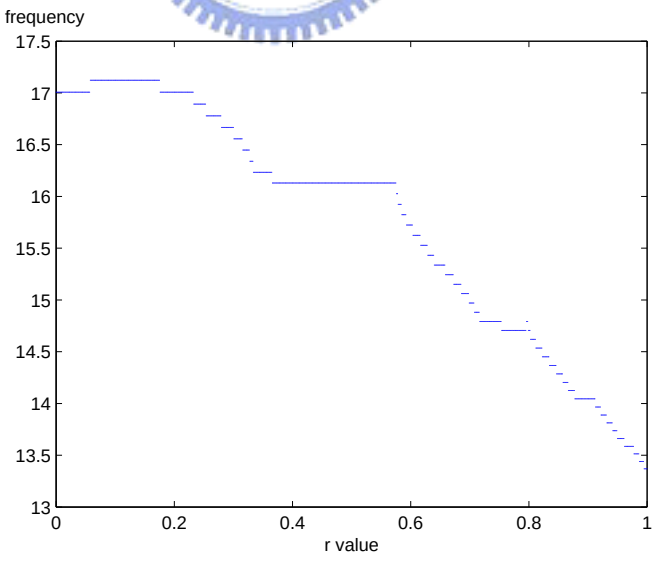

Figure 17. Devil's staircase-like function when $s = 0.5$ and $r \in (0, 1)$

4 Some numerical results: PART II

In the previous section, the CNNs we consider are coupled differential equations and there are nonzero connection strength between A_1 and A_2 subsystem. This means that the neuron x_1 in A_1 and x_3 in A_2 have influence upon each other, so the direction of connection strength is both-side. From the result stated in subsection 3.2 we know that a chaotic attractor occurs only for suitable r and s, and r should be much larger than s.

Motivated by the 1-dimensional, coupled CNNs, in the following we will consider the solid, uncoupled multi-layer CNNs. We start from two-layer CNNs and present them in subsection 4.1, and generalize this idea to three-layer CNNs next. We have derived some new and interesting results from numerical computations and they will be shown in subsection 4.2 later.

4.1 Two-layer CNN model

After considering the coupled two two-cell CNN model, we will further consider the two-layer CNN model described by the following nonlinear autonomous ordinary differential equations systems:

$$\begin{cases} \dot{x_1} &= -x_1 + p_1 y_1 + s_1 y_2 \ , \\ \dot{x_2} &= -x_2 + r_1 y_1 + p_1 y_2 \ , \\ \dot{x_3} &= -x_3 + p_2 y_3 + s_2 y_4 + b_{13} y_1 + b_{23} y_2 \ , \\ \dot{x_4} &= -x_4 + r_2 y_3 + p_2 y_4 + b_{14} y_1 + b_{24} y_2 \ , \end{cases} \tag{4.1}$$

where x_1, x_2, x_3 and x_4 present the voltages of the neurons, and the output function of a neuron is a piecewise-linear neuron-activation function as well. The model consists of two layers and there are two neurons in each layer; we call the subsystem formed by x_1 and x_2 layer 1 and the subsystem formed by x_3 and x_4 layer 2. Note that we denote b_{ij} to stand for the connection strength from the i-th neuron to j-th neuron to avoid confusing. For clarity, we use a chart to signify the relations between these four neurons (cf. Figure 16).

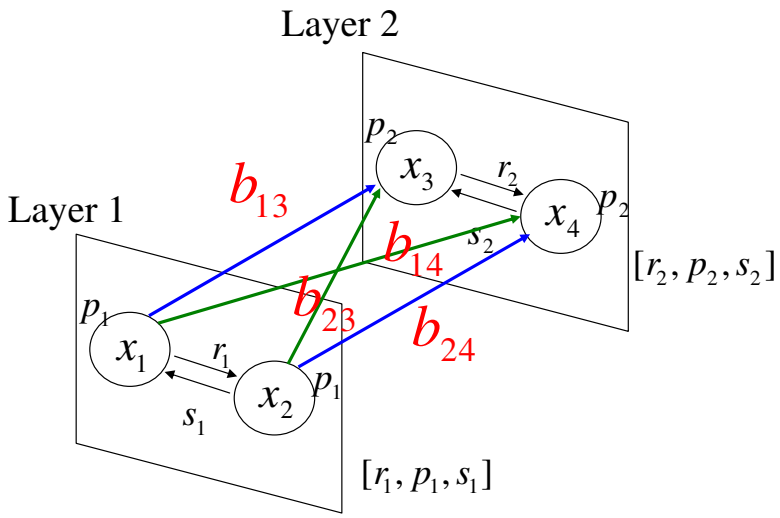

Figure 16. The two-layer autonomous CNN model

From the system (4.1) itself, we know that y_1 and y_2 are both taken to be the input functions of x_3 and x_4. Moreover, the arrowheads in figure 16 also indicate that there are single-direction effects from layer 1 to layer 2. So, being different from models in Section 3, the system (4.1) is an uncoupled system in practice since the layer 2 does not influence layer 1 at all. From another point of view, we attempt using layer 1 to drive layer 2 and observe what happened in layer 2. At present the system (4.1) involves 10 parameters: $r_1, p_1, s_1, r_2, p_2, s_2, b_{13}, b_{23}, b_{14}$ and b_{24}. Generally speaking, for convenience, we simplify the model by letting $b_{14} = b_{23} = b_{24} = 0$ in later discussion. The simplified model and the corresponding figure are expressed as following.

$$\begin{cases} \dot{x_1} &= -x_1 + p_1 y_1 + s_1 y_2 \ , \\ \dot{x_2} &= -x_2 + r_1 y_1 + p_1 y_2 \ , \\ \dot{x_3} &= -x_3 + p_2 y_3 + s_2 y_4 + b_{13} y_1 \ , \\ \dot{x_4} &= -x_4 + r_2 y_3 + p_2 y_4 \ , \end{cases} \tag{4.2}$$

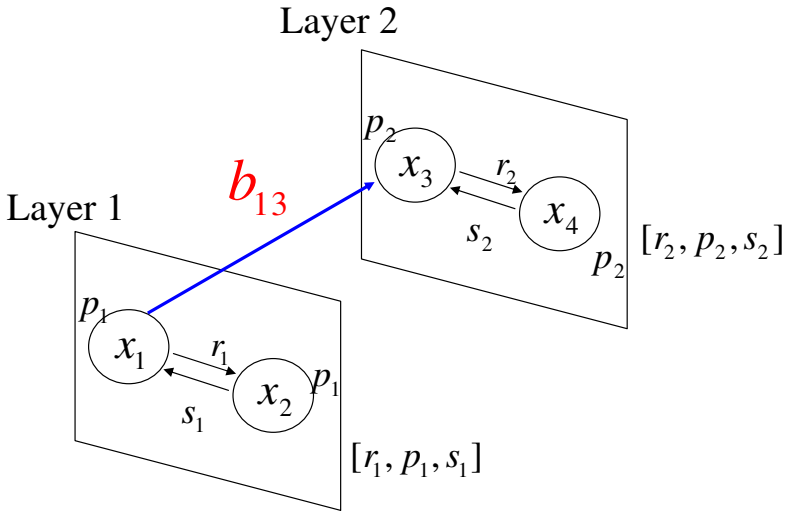

Figure 17. The simplified two-layer autonomous CNN model

Numerical results in Section 3 have exhibited a chaotic attractor in some specific parameters in coupled two two-neuron CNN (cf. Figure 11). Following their setting of case 2 in subsection 3.2, we choose $A_1 = [2.9, 1.7, -2.9]$ as template in layer 1, and $A_2 = [1.2, 2, -1.2]$ as template in layer 2. Similarly, when $b_{13} = 3.5$, a chaotic attractor with positive Lyapunov exponent can also be observed in x_3-x_4 plane (cf. Figure 18).

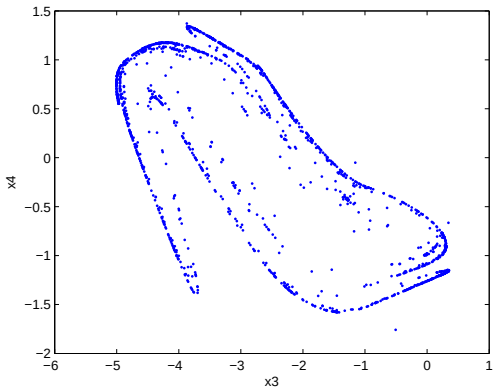

Figure 18. An chaotic attractor in 2-layer CNN when b_{13}=3.5

4.2 Three-layer CNN model

Motivated by two-layer CNN, we continue to consider three-layer CNN model by adding the third layer behind the original case. The model is shown in Figure 19.

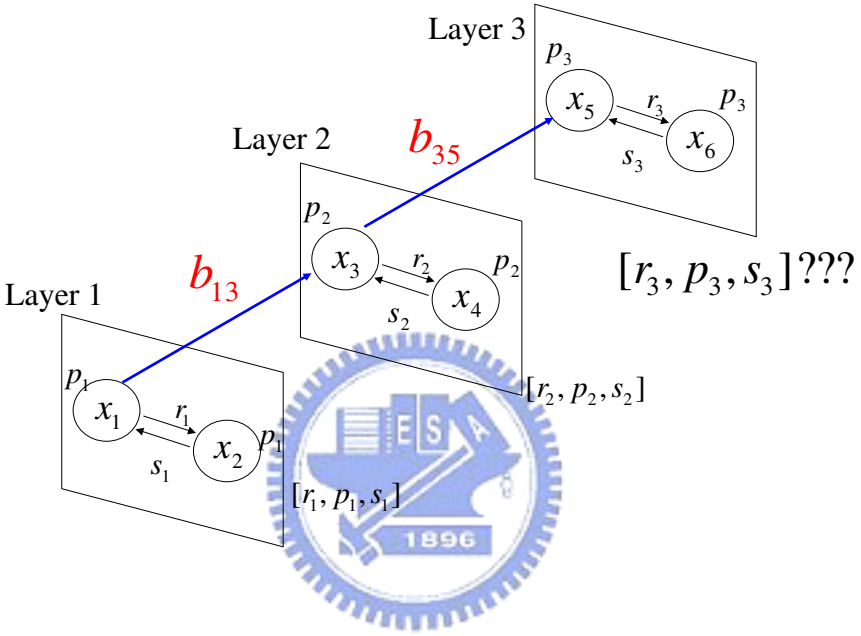

Figure 19. The simplified two-layer autonomous CNN model

Similar to 2-layer case, 3-layer CNN model can be described by the following differential equations.

$$\begin{cases} \dot{x_1} &= -x_1 + p_1 y_1 + s_1 y_2 \ , \\ \dot{x_2} &= -x_2 + r_1 y_1 + p_1 y_2 \ , \\ \dot{x_3} &= -x_3 + p_2 y_3 + s_2 y_4 + b_{13} y_1 \ , \\ \dot{x_4} &= -x_4 + r_2 y_3 + p_2 y_4 \ , \\ \dot{x_5} &= -x_5 + p_3 y_5 + s_3 y_6 + b_{35} y_3 \ , \\ \dot{x_6} &= -x_6 + r_3 y_5 + p_3 y_6 \ , \end{cases} \tag{4.3}$$

From the previous section we know that there is a chaotic attractor occurs in layer 2. Next, we attempt to take the chaotic attractor to drive the periodic solution in layer 3. Although the attractor in layer 2 is chaotic, we can still apply methods to find its average period. This method has been used in physics and engineering widely. We evaluate the average period of chaotic attractor in Figure 18 and the result is around 5.26. So we may divide into two cases for the period of solution generated in layer 3. One is larger than 5.26, and the other one is smaller than 5.26. The possible candidates for template A_3 are listed in table 4.

template A_3	period of $T_{\Lambda 3}$
$[3, 1.2, -3]$	2.55
$[2.8, 1.3, 2.8]$	3.00
$[2.5, 1.5, -2.5]$	4.00
$[2, 1.5, -2]$	5.04
$[2.1, 1.7, -2.1]$	5.64
$[2.4, 2, -2.4]$	6.10
$[1, 1.1, -1]$	7.00
$[1.5, 1.9, -1.5]$	10.08
$[1.2, 1.7, -1.2]$	11.02
$[1, 1.6, -1]$	12.50
$[1.1, 1.8, -1.1]$	14.39
$[1.2, 2, -1.2]$	17.01
$[1.1, 2, -1.1]$	21.92
$[1, 1.9, -1]$	22.25

Table 4. The various templates and its corresponding period

In order to study how the chaotic attractor influence various periodic solution with different period, we classify them according to periods. For example, in the following, we select four kinds of templates; case one is smaller than 5, and case two is nearly 5, and case three is larger than 5, and the last case is far larger than 5. From the candidates in table 4, we select a representative template in each case and arrange them in table 5.

	template A_3	T_{A_3}	result
Case 1	$[3, 1.2, -3]$	2.55	Figure 20
Case 2	$[1, 1.1, -1]$	7.00	Figure 21
Case 3	$[1, 1.6, -1]$	12.50	Figure 22
Case 4	$[1, 1.9, -1]$	22.25	Figure 23

Table 5. The representative templates with different periods

In the following numerical results, we hold $b_{13} = 3.5$ and template A_3 fixed in each case, so the only parameter is b_{35}. By varying b_{35} we can see the evolution of the new chaotic attractor occurs in x_5-x_6 plane. From the figure 20 to 23, it seems that chaotic attractor are preserved when we take the chaotic attractor to drive the periodic solution. The Lyapunov exponents in each cases are computed, and result ensures that the system is chaotic. We have tried our best to investigate the phenomena about 3-layer CNN, however, there are still many unknowns. Next the follow-up we may further consider 4-layer or 5-layer CNN, and expect that we can understand more on the dynamics of multi-layer CNN models in the future.

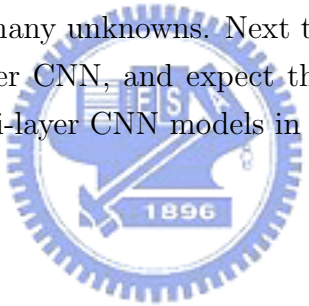

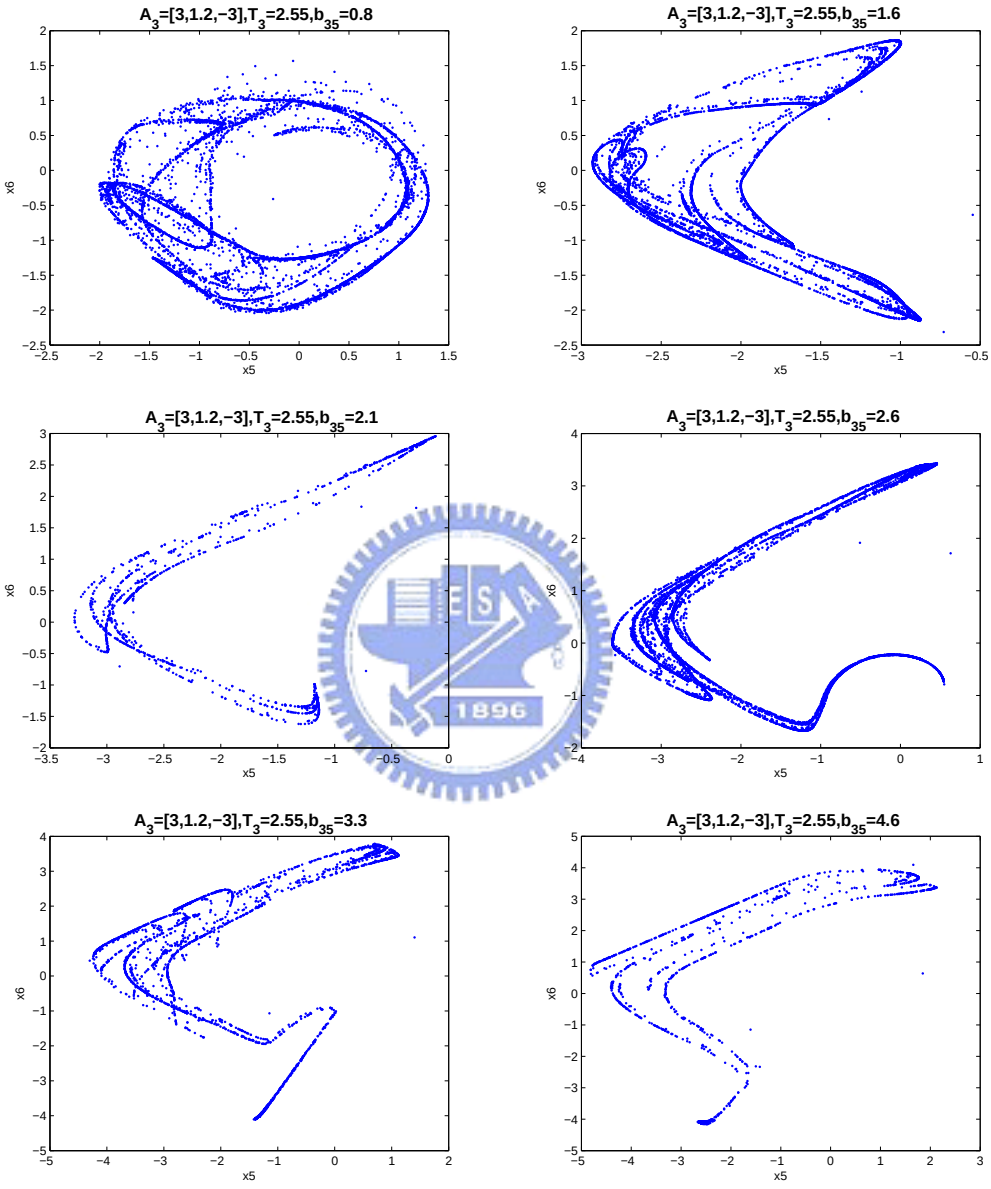

Figure 20. $A_3 = [3, 1.2, -3], T_{A_3} = 2.55$.

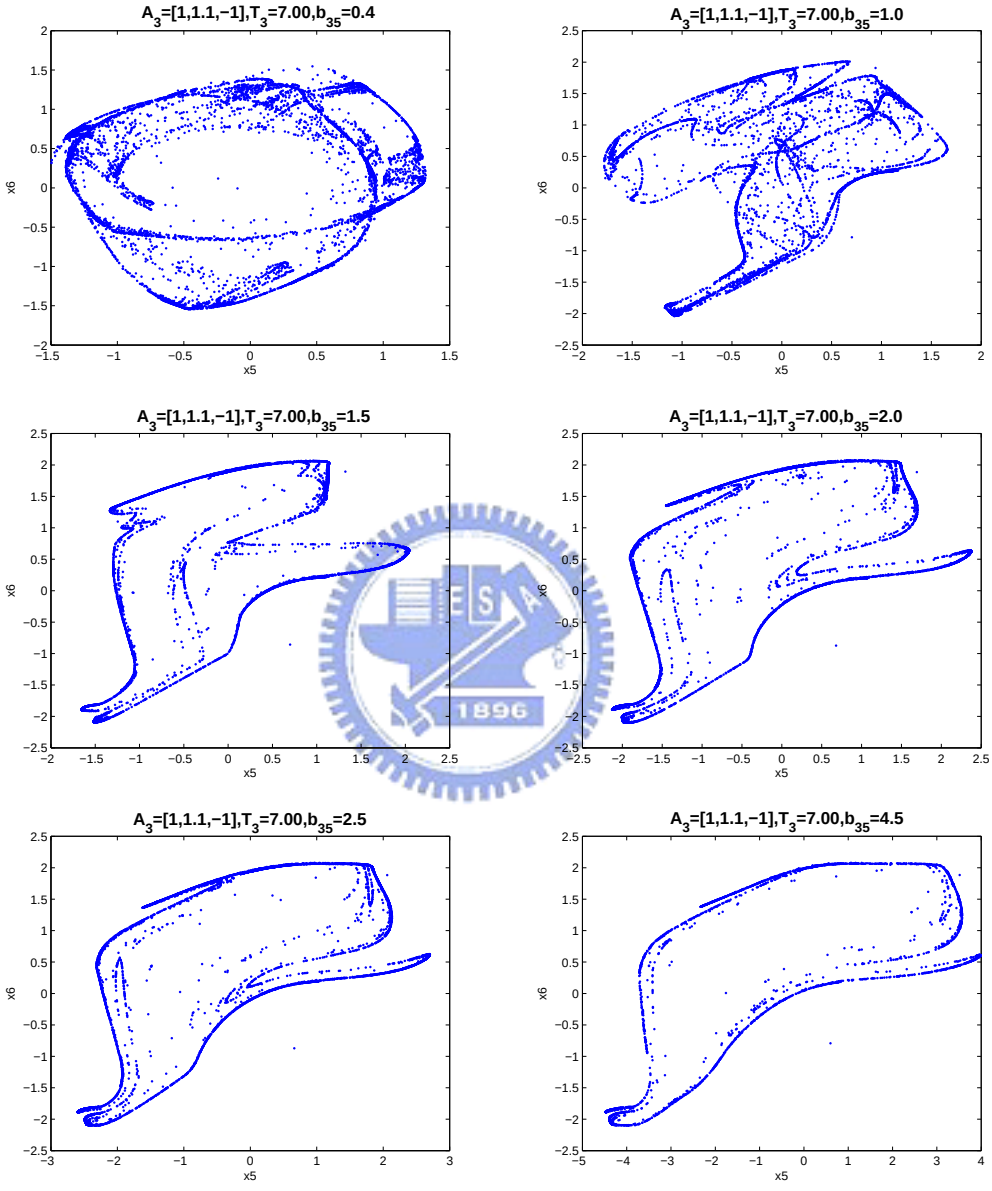

Figure 21. $A_3 = [1, 1.1, -1], T_{A_3} = 7.00$

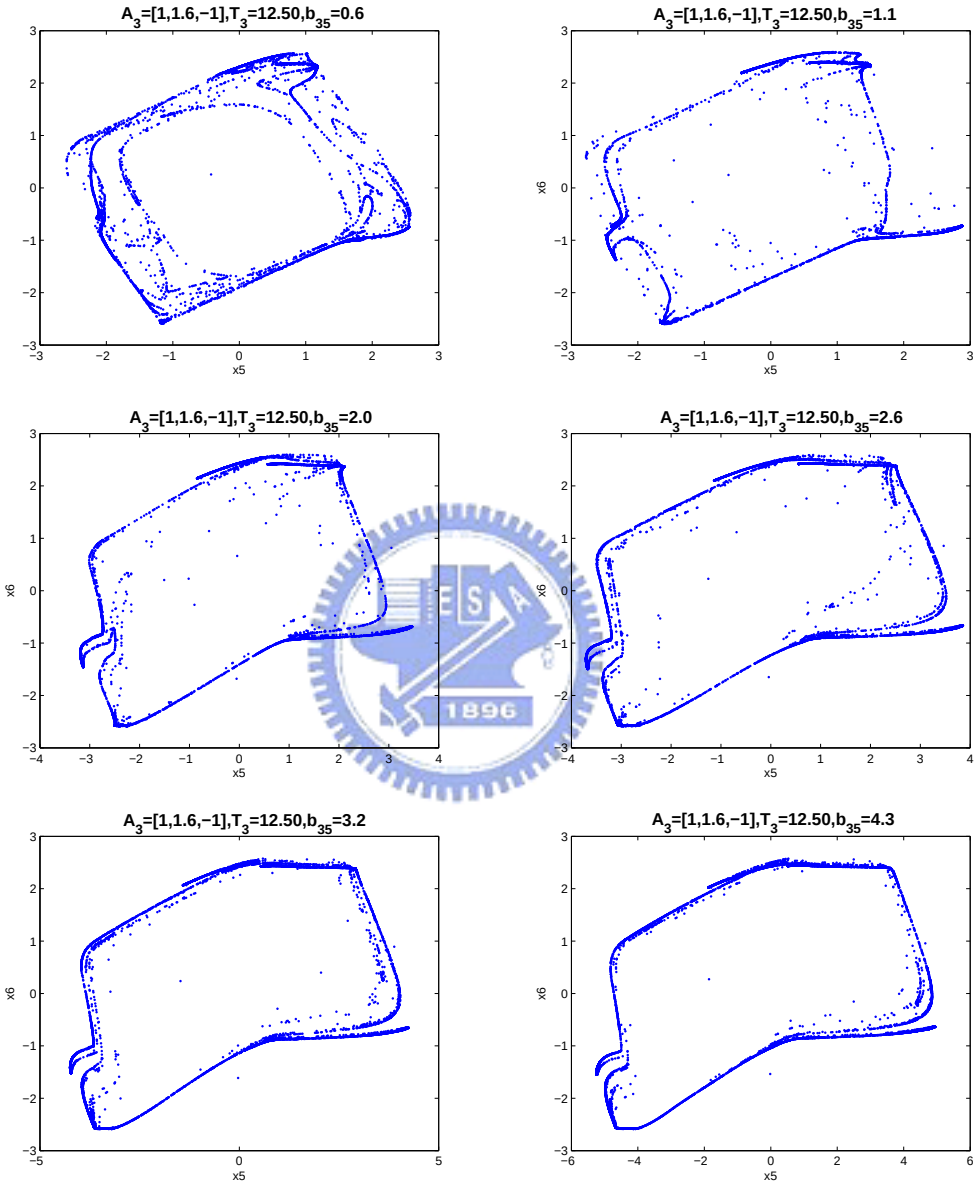

Figure 22. $A_3 = [1, 1.6, -1], T_{A_3} = 12.50$

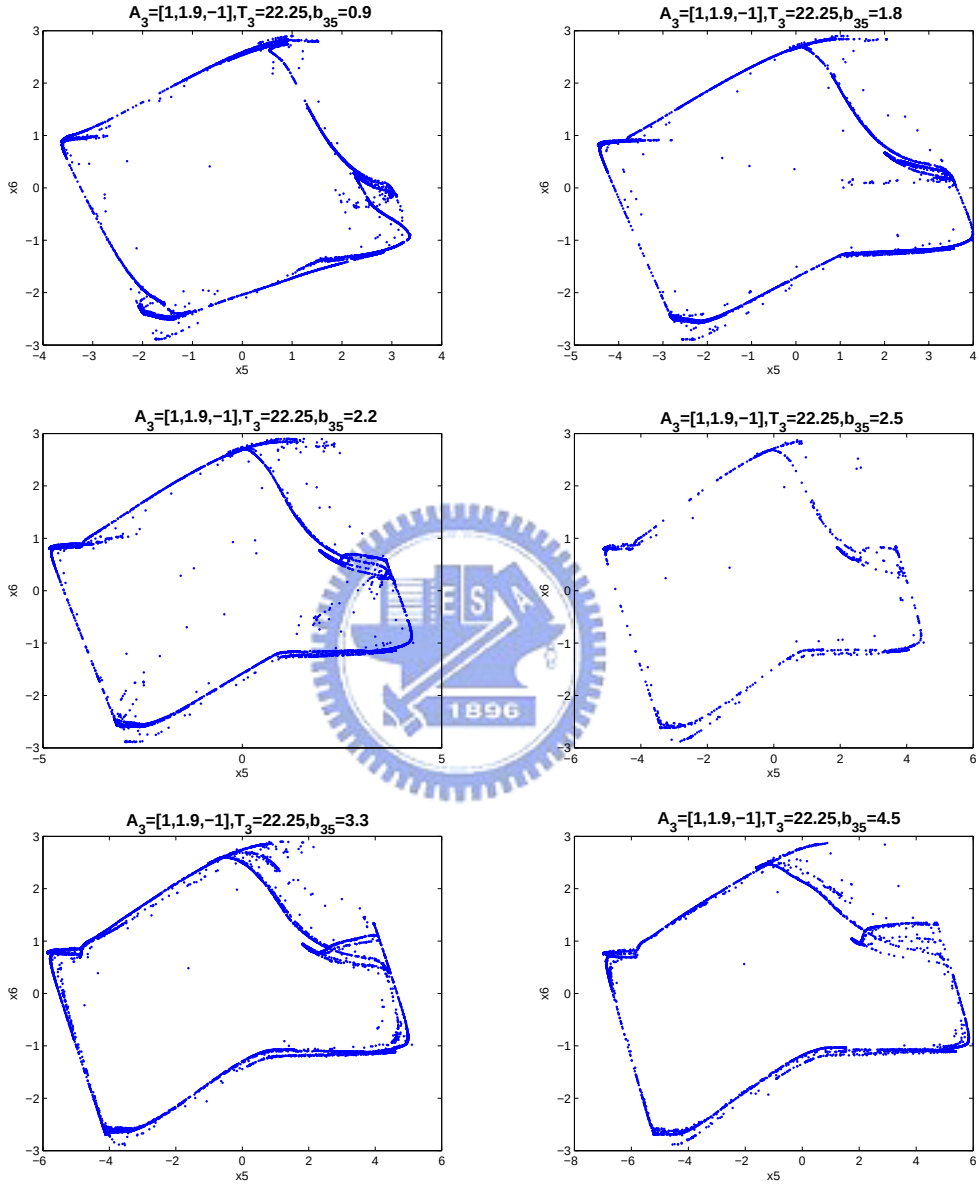

Figure 23. $A_3 = [1, 1.9, -1], T_{A_3} = 22.25$

5 Conclusions and future works

The chaos in cellular neural networks are popular all the time. About the research on the stability and phenomena, researchers proved that a two-neural autonomous networks system will always have no chaotic behavior. However in this thesis, from the four-neuron case combined by two two-neuron cases, a chaotic attractor under suitable parameters is discovered.

Whether two-neuron or four-neuron CNN, we find that when we take the input function with small period to drive the periodic solution with larger period then it is possible to discover the chaos. On the other hand, if we take the periodic solution with larger period to drive the periodic solution with smaller period, then numerical results indicate that there are at most three phenomena: equilibrium, periodic solution and quasi-periodic solution. We have found several possible chaotic attractor in several neural networks models and do qualitative analysis about them in this study, however our discussion was relatively rough. In order to understand complex dynamical behavior of the CNN deeply, rigorous theoretical analysis is needed. We will try our best to deal with them in the future.

To sum up ,we just focus on some typical output function and input function, however, if the output function and input function are varied, other interesting phenomena may occur. There are still much unknown about the CNN model. The CNN we consider is just a simple case, but we can do something about five-neuron, six-neuron in the future works. In other words, we can extend our model to more complicated cases based on the two-neuron and four-neuron CNN models.

References

[1] L. O. Chua and L. Yang, "Cellular neural networks : Theory", *IEEE Trans. Circuit Syst.* **35**(1988a),pp. 1257-1272.

[2] L. O. Chua and L. Yang, "Cellular neural networks : Applications", *IEEE Trans. Circuit Syst.* **35**(1988b),pp. 1273-1290.

[3] L. O. Chua, *CNN : A Paradigm for Complexity*, World Scientific Series on Nonlinear Science, Series A, vol. **31**, World Scientific, Singapore, 1998.

[4] S.-S. Lin and C.-W. Shih, "Complete stability for standard cellular neural networks", *Int. J. of Bifurcation and Chaos*, **9**(1999),pp. 909-918.

[5] C.-W. Shih, "Complete stability for a class of cellular neural networks", *Int. J. of Bifurcation and Chaos*, **11**(2001),pp. 169-177.

[6] J. Juang and S.-S. Lin, "Cellular neural networks: defect pattern and spatial chaos", preprint.

[7] J. Juang and S.-S. Lin, "Cellular neural networks: mosaic pattern and spatial chaos", *SIAM J. Appl. Math.* **60**(2000),pp. 891-915.

[8] C.-H. Hsu, J. Juang, S.-S. Lin and W.-W. Lin, "Cellular Neural Networks: local patterns for general templates", *Int. J. of Bifurcation and Chaos*, **10**(2000),pp. 1645-1659.

[9] C.-H. Hsu and S.-S. Lin, "Spatial disorder of Cellular Neural Networks", *Japan J. of Industrial and Applied Mathematics* **19**(2001),pp. 143-161.

[10] J.-C. Ban, K.-P. Chien, C.-H. Hsu and S.-S. Lin, "Spatial disorder of Cellular Neural Networks - with asymmetric output function:, *Int. J. of Bifurcation and Chaos*, **11**(2001),pp. 2085-2095.

[11] J.-C. Ban, C.-H. Hsu and S.-S Lin, "Spatial disorder of Cellular Neural Networks-with biased term", *Int. J. of Bifurcation and Chaos*, **12**(2002),pp. 525-534.

[12] S.-S. Lin and T.-S. Yang, "Spatial entropy of one dimensional cellular neural network", *Int. J. of Bifurcation and Chaos*, **10**(2000),pp. 2129-2140.

[13] S.-S. Lin and T.-S. Yang, "On the spatial entropy and patterns of two-dimensional cellular neural network", *Int. J. of Bifurcation and Chaos*, **12**(2002),pp. 115-128.

[14] G. Manganaro, P. Arena and L. Fortuna, *Cellular neural networks :chaos, complexity, and VLSI processing*, Springer, 1999.

[15] M. Hänggi and L. O. Chua, *Simulation of RTD-based CNN cells*, Memorandum UCB/ERL M00/51, Electronic Research Laboratory, University of California, Berkeley, 2000.

[16] P. Thiran, *Dynamics and Self-Organization of Locally Coupled Neural Networks*, Press Polytechniques et Universitaires Romandes, Lausanne, Switzerland, 1997.

[17] L. O. Chua and T. Roska, *Cellular Neural Networks and Visual Computing : Foundation and Applications.*, Combridge University Press, 2002.

[18] P. Thiran, K. R. Crounse, L. O. Chua and M. Hasler, "Pattern formation properties of autonomous cellular neural networks,", *IEEE Trans. Circuits and Systems* **42**(1995),pp. 757-774.

[19] F. Zou and J. A. Nossek, "A chaotic attractor with Cellular Neural Networks",*IEEE Trans. Circuits Syst.* **38**(1991),pp. 811-812.

[20] F. Zou and J. A. Nossek, "Bifurcation and chaos in Cellular Neural Networks",*IEEE Trans. Circuits Syst.* **40**(1993),pp. 166-173.

[21] F. Zou, A. Katérle and J. A. Nossek, "Homoclinic and heteroclinic orbits of the three cells Cellular Neural networks",*IEEE Trans. Circuits Syst.* **40**(1993),pp. 843-848.

[22] S.-S. Lin, W.-W. Lin and T.-H. Yang, "Bifurcation and chaos in two-cell cellular neural networks", *Int. J. of Bifurcation and Chaos*, **14**(2004),pp. 3179-3204.

[23] C.-H. Hsu, S.-Y. Yang, T.-H. Yang and T.-S. Yang, "On periodic solutions of a two-neuron network system with sigmoidal activation functions", to appear in *Int. J. of Bifurcation and Chaos*, 2004.

[24] T. S. Parker and L. O. Chua, *Practical numerical algorithms for chaotic systems.*, Springer-Verlag, 1989.

[25] K. T. Alligood, T. D. Sauer and J. A. Yorke, *Chaos, an introduction to dynamical system*, Springer, 1997.

[26] E. Fehlberg, "Low-order classical Runge-Kutta formulas with stepsize control", NASA TR R-315, 1968.

[27] L. Perko, *Differential equations and dynamical systems*, Springer, 1996.